Technical University of Denmark

DTU

Impact of multicomponent ionic transport on pH fronts propagation in saturated porous media

Muniruzzaman, Muhammad; Rolle, Massimo

[Link back to DTU Orbit](#)

DTU Library
Technical Information Center of Denmark

RESEARCH ARTICLE

Key Points:
- Propagation of pH fronts strongly depends on electrostatic interactions
- Clear coupling of dispersive ionic fluxes also in advection-dominated systems
- Multicomponent ionic transport modeling necessary to interpret the experiments

Impact of multicomponent ionic transport on pH fronts propagation in saturated porous media

Muhammad Muniruzzaman[1] and Massimo Rolle[1,2]

[1]Center for Applied Geosciences, University of Tübingen, Tübingen, Germany, [2]Department of Environmental Engineering, Technical University of Denmark, Lyngby, Denmark

Abstract We investigate the propagation of pH fronts during multicomponent ionic transport in saturated porous media under flow-through conditions. By performing laboratory bench-scale experiments combined with numerical modeling, we show the important influence of Coulombic effects on proton transport in the presence of ionic admixtures. The experiments were performed in a quasi two-dimensional flow-through setup under steady-state flow and transport conditions. Dilute solutions of hydrochloric acid with $MgCl_2$ (1:2 strong electrolyte) were used as tracer solutions to experimentally test the effect of electrochemical cross coupling on the migration of diffusive/dispersive pH fronts. We focus on two experimental scenarios, with different composition of tracer solutions, causing remarkably different effects on the propagation of the acidic fronts with relative differences in the penetration depth of pH fronts of 36% between the two scenarios and of 25% and 15% for each scenario with respect to the transport of ions at liberated state (i.e., without considering the charge effects). Also differences in the dilution of the distinct ions plumes up to 28% and 45% in experiment 1 and 2, respectively, were measured at the outflow of the flow-through system. The dilution of the pH plumes also changed considerably (26% relative difference) in the two flow-through experiments only due to the different composition of the pore water solution and to the electrostatic coupling of the ions in the flow-through setups. Numerical transport simulations were performed to interpret the laboratory experiments. The simulations were based on a multicomponent ionic formulation accurately capturing the Coulombic interactions between the transported ions in the flow-through system. The results of purely forward simulations show a very good agreement with the high-resolution measurements performed at the outlet of the flow-through setup and confirms the importance of charge effects on pH transport in porous media.

1. Introduction

The correct quantification of pH distribution is of utmost importance in various areas of subsurface research including the study of groundwater acidification [e.g., *Moss and Edmunds*, 1992; *de Caritat*, 1995; *Hansen and Postma*, 1995; *Donovan et al.*, 1997; *Kjøller et al.*, 2004; *Fest et al.*, 2005, 2007; *Franken et al.*, 2009], sorption-desorption, and surface complexation of trace metals onto mineral surfaces [e.g., *Davis and Kent*, 1990; *Zachara et al.*, 1991; *Kent et al.*, 2000; *Davis et al.*, 2004; *Prigiobbe and Bryant*, 2014], ion exchange [e.g., *Griffioen*, 1993; *Appelo*, 1994], redox-controlled reaction fronts [e.g., *Engesgaard and Kipp*, 1992], as well as mineral equilibria and reactive transport [e.g., *Maher et al.*, 2006; *Li et al.*, 2007, 2014; *Molins et al.*, 2012; *Redden et al.*, 2014; *Haberer et al.*, 2015]. In particular, groundwater acidification, mainly caused by acid rain precipitation, has been identified as a serious problem especially in aquifers with sediments containing low pH buffering capacity [*Edmunds and Kinniburgh*, 1986; *Hansen and Postma*, 1995; *Kjøller et al.*, 2004; *Franken et al.*, 2009]. In such systems, the acidic recharge reaches the saturated zone where the pH front penetrates downward and mixes with the underlying ambient groundwater. Key processes leading to vertical mixing are molecular diffusion and transverse hydrodynamic dispersion. Diffusion of charged species is significantly affected by electrochemical migration effects induced by the charge of dissolved species and/or mineral surfaces [e.g., *Vinograd and McBain*, 1941; *Lasaga*, 1979; *Van Cappellen and Gaillard*, 1996; *Liu*, 2007; *Appelo and Wersin*, 2007; *Steefel and Maher*, 2009]. Multispecies diffusion models, which are traditionally represented by Nernst-Planck formulations, are used to predict diffusive fluxes under such conditions [e.g., *Boudreau et al.*, 2004; *Liu et al.*, 2004; *Appelo and Wersin*, 2007; *Li et al.*, 2008]. These models allow capturing interspecies interactions by preserving local charge balance, and thus represent valuable tools to accurately

describe multicomponent conservative and reactive solute transport occurring in both laboratory and field-scale domains [e.g., *Vinograd and McBain*, 1941; *Giambalvo et al.*, 2002; *Appelo et al.*, 2008, 2010; *Liu et al.*, 2011]. In two recent contributions, we studied multicomponent ionic transport in saturated porous media and we showed that, in addition to purely diffusive processes, the charge-induced Coulombic interactions significantly affect transverse hydrodynamic dispersion and the transport of ionic species in advection-dominated homogeneous and heterogeneous flow-through systems [*Rolle at al.*, 2013a; *Muniruzzaman et al.*, 2014]. These studies were restricted to transport of soluble salts and, to the best of our knowledge, no investigation has yet focused on the effects of charge interactions on pH-front propagation in saturated porous media under flow-through conditions.

The main objective of this work is to study the evolution of diffusive/dispersive pH fronts in the presence of an ionic admixture during conservative solute transport in porous media. To investigate the macroscopic impact of electrostatic effects on acidic front migration under flow-through conditions, we performed quasi two-dimensional bench-scale experiments in a saturated homogeneous porous domain and studied the transport of acidic plumes, undergoing transverse mixing with pure water, under different compositions of the injected electrolyte solution. The experimental results were quantitatively interpreted with a two-dimensional multicomponent transport model taking into account the effects of ionic interactions on pH distribution. The multicomponent simulations allowed us to explain the experimental observations and to quantify the specific components of the transverse dispersive fluxes, including the electromigration term due to the electrostatic coupling between the different ionic species. Our flow-through experiments and modeling results show that the impact of electrostatic microscopic effects is remarkable and causes macroscopic variations in pH-front development and dilution of acidic plumes that are significantly controlled by the presence and concentration of other electrolytes in the pore water solution.

2. Equations of Multicomponent Ionic Transport

Multicomponent diffusion models for species with nonzero charge are commonly derived based on the Nernst-Planck equation [*Bard and Faulkner*, 2001]. The formulations of such models involve the pragmatic extension of Fick's first law by considering an additional charged-induced electrostatic term. In dilute solutions and in the condition of negligible ionic strength gradients, the diffusive flux of an ionic species i in a multicomponent environment is expressed as [*Lasaga*, 1979; *Cussler*, 2009]:

$$J_i = -D_i \nabla C_i - D_i \frac{z_i F}{RT} C_i \nabla \Phi \quad i = 1, 2, 3, ..., N \tag{1}$$

where C_i is the concentration, z_i is the charge, D_i is the self-diffusion coefficient, F is the Faraday's constant, R is the ideal gas constant, T is the absolute temperature, Φ is the electrostatic potential, and N is the number of species in solution. Equation (1) indicates that the flux of a charged species, i, is not only driven by its own concentration gradient but also by the electrical field created by the movement of different ions present in the system.

A detailed derivation of the governing equations for the multicomponent diffusion problem can be found in previous studies [e.g., *Ben-Yaakov*, 1972; *Lasaga*, 1979, *Van Cappellen and Gaillard*, 1996; *Boudreau et al*, 2004; *Appelo and Wersin*, 2007; *Liu et al.*, 2011]. Key steps in the derivation are the physical constraints associated with the electroneutrality of the aqueous solution: (i) local preservation of charge balance in all spatial locations ($\sum_{i=1}^{N} z_i C_i = 0$), and (ii) the absence of electrical current ($\sum_{i=1}^{N} z_i J_i = 0$). Using these constraints, the gradient of electrical potential, $\nabla \Phi$ in equation (1) can be expressed in terms of easily quantifiable parameters such as concentration and charge of the ions in solution as well as their self-diffusion coefficients:

$$\nabla \Phi = \frac{-\sum_{i=1}^{N} (z_i D_i \nabla C_i)}{\sum_{i=1}^{N} (z_i^2 F D_i C_i)/RT} \tag{2}$$

After substitution of equation (2) into equation (1), the diffusive flux readily reduces solely to a function of diffusion coefficients, charge and concentration of the ions in solution, and concentration gradients:

$$J_i = -D_i \nabla C_i + \frac{z_i D_i C_i}{\sum\limits_{j=1}^{N} \left(z_j^2 D_j C_j \right)} \sum_{k=1}^{N} \left(z_k D_k \nabla C_k \right) \tag{3}$$

Equation (3) can be further rearranged in a more compact notation by introducing a matrix of interdiffusion coefficients, cross-coupling fluxes, and concentration gradients of the dissolved species. The multicomponent formulation of diffusive processes has been adopted and shown to be relevant in numerous studies in the geochemical and water research literature [e.g., *Lasaga*, 1979; *Van Cappellen and Gaillard*, 1996; *Giambalvo et al.*, 2002; *Boudreau et al.*, 2004; *Liu et al.*, 2004, 2011; *Appelo and Wersin*, 2007].

In flow-through systems, solute mass exchange also depends on the advective movement of the fluid. Therefore, under such conditions, hydrodynamic dispersion coefficients should be considered in the derivation of the multicomponent transport problem in porous media [*Rolle at al.*, 2013a; *Muniruzzaman et al.*, 2014]. By substituting the multicomponent dispersive fluxes (formally similar to equation (3)) into the classical advection-dispersion equation, the governing transport equation of ionic species in saturated porous domain takes the form:

$$\frac{\partial C_i}{\partial t} = -\mathbf{v} \cdot \nabla C_i + \nabla \cdot \left(\sum_{j=1}^{N} \mathbf{D}_{ij} \nabla C_j \right) \tag{4}$$

where t is time, $\mathbf{v}$ is the velocity vector, and $\mathbf{D}_{ij}$ is the dispersion tensor. In a two-dimensional system oriented along the principal flow direction, the entries of $\mathbf{D}_{ij}$ are $\mathbf{D}_{ij}^L$ and $\mathbf{D}_{ij}^T$, which represent the longitudinal and transverse cross-coupled dispersion coefficients [*Muniruzzaman et al.*, 2014]:

$$\mathbf{D}_{ij}^L = \delta_{ij} D_i^L - \frac{z_i z_j D_i^L D_j^L C_i}{\sum\limits_{k=1}^{N} \left(z_k^2 D_k^L C_k \right)}$$

$$\mathbf{D}_{ij}^T = \delta_{ij} D_i^T - \frac{z_i z_j D_i^T D_j^T C_i}{\sum\limits_{k=1}^{N} \left(z_k^2 D_k^T C_k \right)} \tag{5}$$

where D_i^L is the longitudinal and D_i^T is the transverse component of the hydrodynamic self-dispersion coefficient of species i (i.e., when the ion is "liberated" from the other charged species in solution), δ_{ij} is the Kronecker symbol which has a value of 1 when $i=j$ or 0 when $i \neq j$. The combination of equations (4) and (5) ensures that the movement of a specific ion depends on its own dispersion coefficient and concentration gradient (first terms in equation (5)) as well as on the properties and concentration gradients of other charged species in solution (second terms in equation (5)).

The general formulation of the multicomponent transport problem (equations (1)–(5)) reduces to the classical advection-dispersion equation for noncharged species, since all the electrostatic cross-coupling terms in equation (5) drop out.

3. Experimental Setup

The experiments were performed in a quasi two-dimensional flow-through setup in a homogeneous porous medium. The flow-through chamber has inner dimensions of 100 cm × 19 cm × 1 cm (L × H × W) and is equipped with 24 ports both at the inlet and at the outlet (Figure 1). These ports, constructed with Alltech rubber septa pierced with hollow injection needles, are directly connected to two 24 channel high-precision peristaltic pumps (ISMATEC IPC-N24, Ismatec, Glattburg, Switzerland) through Fluran HCA pump tubings (inner diameter 0.64 mm; Ismatec, Glattburg, Switzerland). The porous medium was prepared by filling the flow-through chamber with glass beads with grain diameter in the range 1.00–1.50 mm (Sartorius AG, Göttingen, Germany). A wet-packing procedure was followed by maintaining the water level always above the upper limit of the porous medium to avoid possible air entrapment [*Haberer et al.*, 2012]. The pumps, calibrated before each experiment, allowed establishing a uniform horizontal flow field and the small spacing between the ports (5 mm) allowed high-resolution sampling of the injected tracer solutions. The experiments were performed in a temperature controlled room at a temperature of 20°C.
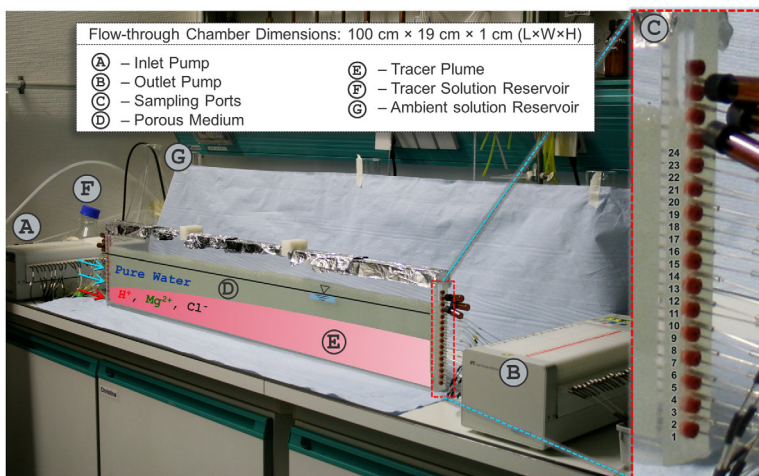
Figure 1. Laboratory flow-through setup. The red-shaded area represents the steady-state plume of ionic species (H^+, Mg^{2+}, and Cl^-) injected from the eight bottom inlet ports. The inset shows the high-resolution sampling at the outlet of the flow-through chamber.

The flow-through experiments were initiated by injecting tracer solutions through eight injection ports at the bottom of the chamber (port 1–8; 0–4 cm from the bottom) and an ambient solution of ultra-pure Milli-Q water (Millipore, MA, USA) through the remaining inlet ports. Such solutions were continuously injected until steady-state transport conditions were achieved and samples were taken afterwards at all 24 outlet extraction ports (Figure 1).

The acidic solutions injected from the bottom inlet ports contained HCl and $MgCl_2$, a strong 1:2 electrolyte injected at similar and hundredfold concentrations relative to HCl in different experimental runs. Mg^{2+} and Cl^- concentrations were measured by ion-chromatography (Dionex Dx-120, Fisher Scientific, Schwerte, Germany) and pH measurements were performed by pH electrode (ORION 8103BN, Thermo Fisher Scientific Inc., USA). For each experimental run, duplicate measurements at each outlet port were taken. Additionally, the flow rate at each port was determined gravimetrically, by collecting and weighing the effluent volume for a given period of time. The flow rate measurement was always carried out after sampling for the ion concentration measurements. The transport experiments were performed in an advection-dominated regime, at a seepage velocity of 0.8 m/d. The parameters summarizing the main features of the flow-through setup as well as the flow and transport properties are reported in Table 1.

The values of the ion diffusion coefficients reported in Table 1 are important for this study. Such values represent the aqueous self-diffusion coefficients of the ionic species under the experimental conditions of the flow-through experiments. It is interesting to notice the variability of the diffusivity constants which depend not only on the size of the different ions but also on the electrostatic interactions of the ions with the polar solvent. These effects cause a cohort of solvation molecules, denoted as first solvation shell, to follow the movement of the ions [*Møller et al.*, 2005]. Particularly striking is the value of D^{aq} for the hydrogen ion, which is more than one order of magnitude larger than the diffusivity of the other cations in solution. The large diffusivity of H^+ cannot be explained by hydrodynamic considerations and arise from specific "Grotthuss-type" mechanisms resulting in proton hopping through a chain reaction between water molecules [*Cussler*, 2009]. These properties are of

Table 1. Summary of Geometry and Flow and Transport Parameters of the Laboratory Experimental System

Experimental Settings	
Flow-through chamber inner dimensions (L×H×W) (cm)	$100 \times 19 \times 1$
Number of inlet/outlet ports used	23/24
Port spacing (mm)	5
Grain diameter of the porous matrix, d (mm)	1.00–1.50
Hydraulic conductivity, K (m/s)	1.27×10^{-2}
Average horizontal flow velocity, v (m/d)	0.8
Average porosity, θ (−)	0.41

Diffusion Coefficients	D^{aq} (m²/s)[a]
H^+	8.65×10^{-9}
Mg^{2+}	0.63×10^{-9}
Cl^-	1.81×10^{-9}

[a]Values from *Lasaga* [1998] at 18°C, and corrected for temperature and viscosity changes of the experimental conditions at 20°C.

Table 2. Chemical Composition of the Inlet Solutions in the Flow-Through Experiments

Parameter	Scenario 1	Scenario 2
pH	3.8	4.1
Mg^{2+} concentration, C_{Mg2+} (mM)	0.15	12.0
Cl^- concentration, C_{Cl-} (mM)	0.46	24.1
C_{H+}/C_{Mg2+} (−)	1.14	0.007
Ionic strength (M)	6×10^{-4}	3.61×10^{-2}

primary importance for the propagation of pH fronts that can advance at a considerably higher speed than the other ions in the pore water solution. As illustrated in this study, the ions in solution have the capability to strongly influence the displacement of the hydrogen ions.

The laboratory experiments were performed considering a ternary electrolyte system containing two cations (H^+, Mg^{2+}) and a common anion Cl^-. In particular, two experimental scenarios with different composition of the inlet solutions were tested: (i) Scenario 1: transport of a HCl and $MgCl_2$ solution with similar concentration of the two cations (i.e., $C_{H+}/C_{Mg2+} \approx 1$) in ambient Milli-Q water, and (ii) Scenario 2: transport of a HCl and $MgCl_2$ solution with excess of $MgCl_2$ (i.e., $C_{H+}/C_{Mg2+} \approx 0.01$) in ambient Milli-Q water. The chemical composition of the inlet solutions in the flow-through experiments is summarized in Table 2.

4. Modeling Approach

A two-dimensional steady-state model for flow and multicomponent transport in saturated porous media has been adopted in the present study. The flow problem for hydraulic head, h, and stream-function, ψ, under steady-state conditions reads as [*Cirpka et al.*, 1999a]:

$$\nabla \cdot (\mathbf{K}\nabla h) = 0$$
$$\nabla \cdot (\mathbf{K}^{-1}\nabla\psi) = 0 \tag{6}$$

where $\mathbf{K}$ is the hydraulic conductivity tensor. Equation (6) is solved numerically by bilinear finite elements on Cartesian grids. Dirichlet boundary conditions are applied at the inlet and outlet boundaries for the head problem, and at the top and bottom boundaries for the stream-function problem.

Under steady-state conditions, the governing equation describing multicomponent solute transport, written in local coordinates x_L and x_T oriented along and perpendicular to the direction of the flow, writes as:

$$v\frac{\partial C_i}{\partial x_L} - \frac{\partial}{\partial x_L}\left(\sum_{j=1}^{N}\mathbf{D}_{ij}^L\frac{\partial C_j}{\partial x_L}\right) - \frac{\partial}{\partial x_T}\left(\sum_{j=1}^{N}\mathbf{D}_{ij}^T\frac{\partial C_j}{\partial x_T}\right) = 0 \tag{7}$$

The transport problem is computed with finite volume method (FVM) on streamline-oriented grids constructed by the approach of *Cirpka et al.* [1999a, 1999b]. The use of such grids oriented along the flow direction reduces numerical errors by avoiding artificial mixing. The system of equations is solved using the direct matrix solver UMFPACK [*Davis and Duff*, 1997] and all associated calculations are performed in MATLAB. A Picard iterative scheme is used to linearize the nonlinear set of transport equations (equation (7)), in which the nonlinearity arises from the electrostatic cross-coupling between the dispersive fluxes of the different ions. A detailed description including the development and validation of the two-dimensional multicomponent dispersion model can be found in *Muniruzzaman et al.* [2014].

To simulate the flow-through laboratory experiments, the two-dimensional model domain (100 cm × 12 cm) is discretized into 100 cells ($\Delta x = 1$ cm) and 120 cells ($\Delta z = 1$ mm) along the longitudinal and transverse dimension, respectively. A constant concentration boundary at the inflow and zero dispersive flux conditions at the remaining boundaries are applied. A key parameter for the accurate representation of the displacement of the different ionic species is the hydrodynamic dispersion coefficient which was parameterized according to a nonlinear compound-specific formulation [*Chiogna et al.*, 2010; *Rolle et al.*, 2012]:

$$D_i = D_i^P + D_i^{aq}\left(\frac{Pe^2}{Pe + 2 + 4\delta^2}\right)^\beta \tag{8}$$

where D_i^P is the pore diffusion coefficient approximated as $D_i^P \approx \theta D_i^{aq}$. Pe is the grain Péclet number defined as, $Pe = vd/D_i^{aq}$, with v and d being the seepage velocity and the grain diameter, respectively. δ is the ratio between the length of a pore channel and its hydraulic radius, and β is an empirical exponent accounting for incomplete mixing in the pore channels. For the transverse dispersion coefficient, which is the key

parameter for steady-state transport, the values of $\delta = 6.2$ and $\beta = 0.5$ were determined in previous multi-tracer experiments and pore-scale simulations performed in the same porous medium used in this study [*Rolle et al.*, 2012; *Hochstetler et al.*, 2013]. The same empirical parameterization was used for the longitudinal dispersion coefficient [*Rolle et al.*, 2013b; *Muniruzzaman et al.*, 2014], with the same value for δ and $\beta = 0.89$, determined in transient pore-scale simulations, even though the longitudinal dispersion term in equation (7) becomes negligible for steady-state transport and continuous injection of the tracer solutions [*Cirpka et al.*, 2011].

The electrostatic coupling between the different charged species in the flow-through setup is performed by implementing the equations of multicomponent ionic interactions described in section 2. A simplified approach was followed, considering exclusively the coupling between the major ions measured in the flow-through experiments (H^+, Mg^{2+}, and Cl^-). Such approach is adequate for the experimental conditions considered in this study, as shown by the excellent agreement of the simulation results with the outcome of PHREEQC [*Parkhurst and Appelo*, 1999] for a 1-D multicomponent diffusion problem described in the supporting information. Instead, more complex aqueous chemistry as well as higher concentrations would require a full coupling of a multidimensional transport simulator with a geochemical code allowing considering the full aqueous speciation reactions as well as the influence of ionic strength and the gradients in the activity coefficients.

5. Results and Discussion

Laboratory experiments were performed considering two different systems of ternary electrolytes, containing two cations (H^+, Mg^{2+}) and a common anion Cl^- (Table 2). The results obtained from these two experimental scenarios are quantitatively analyzed with purely forward 2-D multicomponent simulations based on the approach outlined in section 4.

5.1. Scenario 1: Transport of HCl With Similar Molar Concentration of MgCl₂

In this experiment, a dilute solution containing similar molar concentrations of hydrochloric acid (0.17 mM) and $MgCl_2$ (0.15 mM) was continuously injected through eight inlet ports at the bottom of the flow-through setup; Milli-Q water was injected as ambient solution through the remaining ports. The injected ions underwent conservative multispecies transport through the saturated porous medium until the establishment of steady-state plumes. Figure 2 reports the steady-state concentration profiles for Mg^{2+} and Cl^- as well as the pH profiles measured at high vertical resolution at the outlet of the flow-through domain.

The measured vertical concentration profiles show distinct patterns in transverse displacement of injected species (Figure 2a). Such patterns are substantiated by the multicomponent simulations that show a very good agreement with the measurements of the ion concentrations. The distinct patterns confirm the importance of diffusion and compound-specific dispersion under the advection-dominated regime (i.e., seepage velocity of 0.8 m/d) of the flow-through experiments. As expected from their diffusion coefficients (Table 1), the two cations, fast H^+ and slow Mg^{2+}, show different spreading and the common anion Cl^- has a profile
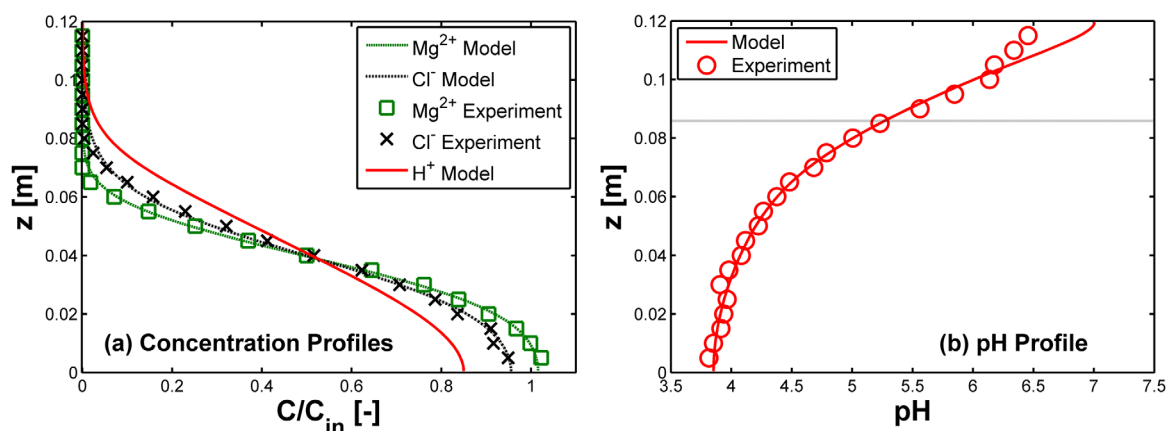

Figure 2. Transverse ion concentrations (a) and pH (b) profiles at the outlet of the flow-through system ($x = 1$ m) for multicomponent transport in Scenario 1 ($C_{H+}/C_{Mg2+} \approx 1$): measured ion concentrations and pH (symbols) and modeling results (lines).

that lies in-between the ones of the cations. The pH was the parameter measured to track the displacement of hydrogen ions. In dilute solution, the pH can be approximated as the negative logarithm of H^+ concentrations. Considering a change of 1.5 pH units from the inlet solution, the results show that at the end of the flow-through system the dispersive pH front has migrated up to a distance of ∼8.6 cm (gray-dotted line in Figure 2b, 4.6 cm above the 4 cm injection zone) from the bottom of the flow-through system. An excellent agreement also exists between the measured pH profiles and the results of the multicomponent transport simulations.

The multicomponent model allows us to map the distinct contributions of steady-state transverse flux components for the different ionic species in solution. In fact, the total dispersive flux, formally identical to equation (1) but considering hydrodynamic dispersion instead of diffusion, consists of an additive contribution of a purely dispersive flux (J_i^{dis}) and an electrochemical migration flux (J_i^{mig}). The latter represents the contribution due to the electrostatic coupling between the charged species:

$$J_i = J_i^{dis} + J_i^{mig} \tag{9}$$

Mapping the different flux contributions is useful to illustrate the coupled transport of the charged species in the multicomponent setup. Maps of the different dispersive flux components are shown in Figures 3a–3i.
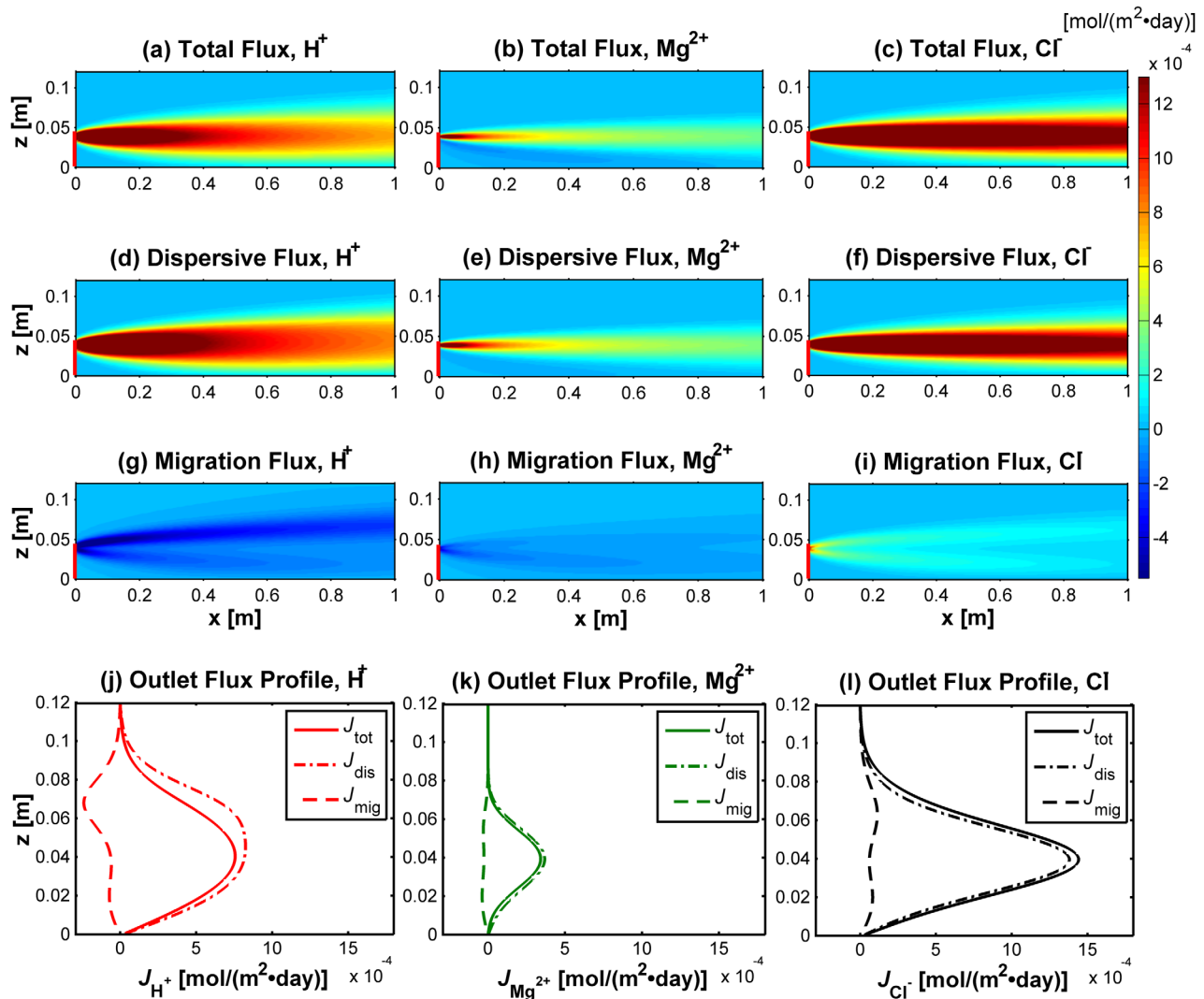

Figure 3. Maps of multicomponent ionic transverse fluxes for Scenario 1: total fluxes (a, b, c), dispersive fluxes (d, e, f), and electrochemical migration fluxes (g, h, i). The bottom plots (j, k, l) show the vertical profiles of multicomponent ionic fluxes at the outlet of the flow-through domain. The vertical red line represents the width of the tracer solution at the inlet. The direction from the core to the fringe (upward) of the plume is considered positive for the calculated fluxes.

The figures illustrates that the total and dispersive fluxes of H^+ are significantly more spread than those of the other ions, in particular of Mg^{2+} (Figures 3a–3f). The electrochemical migration term (J_i^{mig}) shows an interesting distribution with both cations having negative contributions and the anion (Cl^-) having a positive contribution (Figures 3g–3i). Therefore, due to negative electrochemical migration flux components, protons and magnesium ions experience a decrease of their transverse displacement. The situation is opposite for Cl^-, for which a positive electrochemical flux component leads to an enhancement of its transverse flux. As a consequence, in this scenario, both cations slowed down and the anion accelerated compared to their liberated state. This is also evident from the profiles of the transverse fluxes computed at the outlet of the domain (Figures 3j–3l). Notice that for both cations the total flux components have smaller magnitude compared to the purely dispersive flux terms. For Cl^-, instead, both the dispersive and the electrochemical migration fluxes have a positive contribution and add up to a larger total flux. In this scenario, the Coulombic interactions between the different ionic species is particularly effective in limiting the transverse dispersion of the protons whose displacement is considerably reduced compared to the case of transport in the absence of electrostatic effects (i.e., liberated state).

5.2. Scenario 2: Transport of HCl With Excess Molar Concentration of MgCl₂

In this scenario, we investigated the transport of HCl in the presence of excess $MgCl_2$. The tracer solution contained 0.08 mM hydrochloric acid and 12 mM $MgCl_2$. As in the previous experiment, this electrolyte solution was continuously injected through the eight bottom inlet ports and Milli-Q water was injected from the remaining inlet ports. When the plume reached steady state, samples were taken at the 24 outlet ports of the flow-through chamber. The measured and simulated outlet profiles are shown in Figure 4.

Unlike Scenario 1, Mg^{2+} and Cl^-, present in excess concentration, appear to travel together resulting in overlapping concentration profiles (Figure 4a). The hydrogen ion, present in relatively smaller concentration, travels much further compared to the other two ions. This is reflected in a more spread vertical profile with a smaller peak concentration. The pH measurements and simulations shows that the dispersive pH front (1.5 pH units change from the inlet solution) has advanced up to a vertical distance of ~10.2 cm from the bottom (i.e., 6.2 cm above the 4 cm injection zone), at the outlet of the flow-through chamber (Figure 4b). Also in this case, the agreement between the measured profiles and the profiles calculated with the purely forward multicomponent simulations is very good. Also for this scenario, it is illustrative to visualize the different flux components of the ionic plumes in the two-dimensional setup. Figure 5 shows the maps of the steady-state transverse dispersive fluxes and the corresponding profiles at the outlet boundary of the domain.

It is clear from Figures 5a–5c that the total transverse flux for H^+ has a wider distribution compared to the other two ions. This pattern is also consistent with the outlet concentration profiles of the ions shown in Figure 4a. In fact, the transverse flux for H^+ interest a wider portion of the domain and this is reflected also by the higher spreading of the H^+ plume compared to Mg^{2+} and Cl^-. Notable differences between the different ions in solution can be observed also for the dispersive flux components J_i^{dis} (Figures 5d–5f). The electrochemical migration flux distributions (Figures 5g–5i) show an interesting behavior, completely opposite to
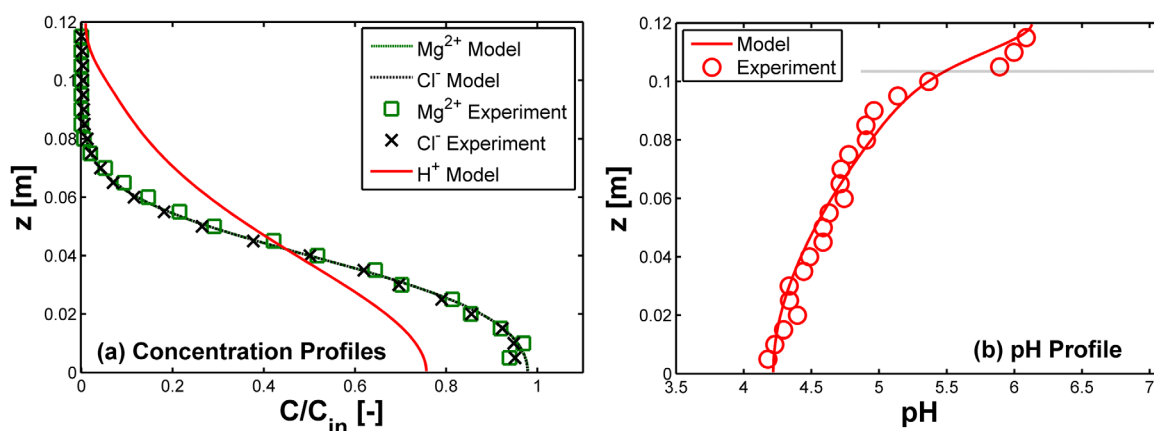

Figure 4. Transverse ion concentrations (a) and pH (b) profiles at the outlet of the flow-through system ($x = 1$ m) for multicomponent transport in Scenario 2 ($C_{H+}/C_{Mg2+} \approx 0.01$): measured ion concentrations and pH (symbols) and modeling results (lines).
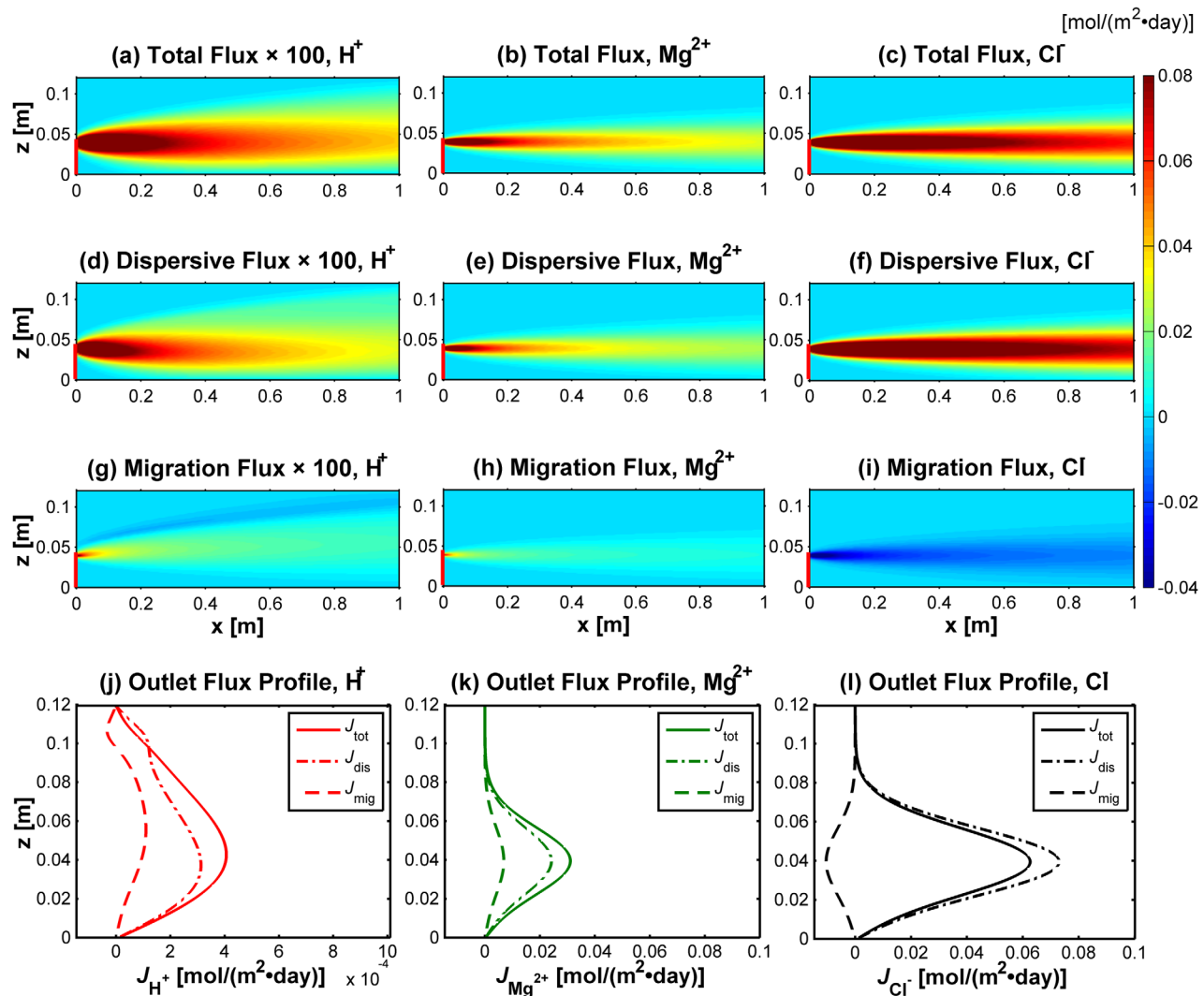
Figure 5. Maps of multicomponent ionic transverse fluxes for Scenario 2: total fluxes (a, b, c), dispersive fluxes (d, e, f), and electrochemical migration fluxes (g, h, i). The bottom plots (j, k, l) show the vertical profiles of multicomponent ionic fluxes at the outlet of the flow-through domain. The vertical red line represents the width of the tracer solution at the inlet. The direction from the core to the fringe (upward) of the plume is considered positive for the calculated fluxes. Additionally, notice that the scale used in the H$^+$ maps and profiles is hundredfold smaller because the absolute concentrations of Mg^{2+} and Cl$^-$ are two orders of magnitude higher compared to the H$^+$ concentration.

the one observed in Scenario 1. In this case, both cations (Mg^{2+} and H$^+$) have a positive contribution and the anion (Cl$^-$) has a negative contribution. This causes an enhancement of Mg^{2+} and a reduction of Cl$^-$ transverse displacements, which leads to the practically identical movement of these two species due to the electrochemical coupling. These effects are also well reflected in the flux profiles computed at the outlet of the domain (Figures 5j–5l). Particularly interesting is to examine the additive contribution of the transverse flux components for the hydrogen ions. Specifically, the electromigration term, $J_{H^+}^{mig}$, shows a positive contribution that accelerates H$^+$ for most of the transverse thickness of the H$^+$ plume. However, at the very edge of the plume ($z > 8$ cm at the outlet cross-section), $J_{H^+}^{mig}$ decreases and becomes negative again (Figures 5g and 5j). This happens because in this outer fringe area, the other two ions (Mg^{2+} and Cl$^-$) are present only in trace amount and the concentration ratio between protons and magnesium ions becomes similar ($C_{H+}/C_{Mg2+} \approx 1$) or even larger ($C_{H+}/C_{Mg2+} > 1$) than in Scenario 1. Consequently, as observed in Scenario 1, a negative contribution of $J_{H^+}^{mig}$ reduces the dispersive flux, $J_{H^+}^{disp}$, and leads to a reduction of transverse movement of H$^+$ in this particular small region of the domain.

The results found in Scenario 1 and 2 clearly show the existence and significance of ionic interactions during acidic plume migration in advection-dominated flow-through systems and how their extent can vary depending on the composition of the same ternary electrolyte system.

5.3. Analysis of the Electrical Potential Gradient

A deeper understanding of the interactions between individual species and insights into the mechanisms of electromigration can be obtained by evaluating the electrical potential gradient produced by different ions on the course of multicomponent transport. The electrical potential gradient is a key term for the electrochemical migration flux (equation (1)) and describes the effect of the additional force, acting on a given ion i, arising from electric fields induced by the different diffusion rates of the charged species in solution [*Lasaga*, 1998]. According to equation (2), the gradient of electrical potential (also known as diffusion potential) in the transverse direction can be calculated as:

$$\frac{\partial \Phi}{\partial x_T} = \frac{-\sum_{i=1}^{N} \left(z_i D_i \frac{\partial C_i}{\partial x_T} \right)}{\sum_{i=1}^{N} \left(z_i^2 F D_i C_i \right) / RT} \tag{10}$$

in which the diffusion coefficients of equation (2) are replaced by transverse hydrodynamic dispersion coefficients for flow-through systems. By considering an electrolyte system with the three major ions considered in our experimental scenarios, the electrical gradient component in the above equation is the additive contribution of the gradients caused by each ion and can be expressed as:

$$\frac{\partial \Phi}{\partial x_T} = \frac{\partial \Phi_{H^+}}{\partial x_T} + \frac{\partial \Phi_{Mg^{2+}}}{\partial x_T} + \frac{\partial \Phi_{Cl^-}}{\partial x_T} \tag{11}$$

Figure 6 represents the calculated electrical gradient and its different components (equation (11)) for both experimental scenarios. Figure 6a also shows that the net electrical potential gradient produced by the movement of different ionic species is negative in Scenario 1. Such net electrical potential gradient consists of a negative contribution for both cations (H^+ and Mg^{2+}) and a positive contribution for the common anion (Cl^-) (Figures 6b–6d). The outlet vertical profiles of ion-specific electrical potential gradients for this experimental scenario are shown in Figure 6e.

In the source zone ($z = 0$–4 cm), the components from the cations ($\frac{\partial \Phi_{H^+}}{\partial x_T}$ and $\frac{\partial \Phi_{Mg^{2+}}}{\partial x_T}$) tend to counterbalance the anionic component, $\frac{\partial \Phi_{Cl^-}}{\partial x_T}$. However, due to the differences in their diffusivities, the electrostatic gradient develops in the fringe area. The gradient in the electrostatic potential generates an electrical field, under which electrical forces are exerted on the dissolved charged species in the solution. The magnitude of the force imposed on individual species is dependent on the charge of the dissolved species and the overall electrical gradient. The flux due to the electrical gradient for an individual species is directly proportional to the force active on that species and the species' concentration [*Probstein*, 1989]. As a result, the active electric field enforces the dissolved ionic species' diffusive movement (electromigration) in the solution to maintain electroneutrality. In particular, for this specific experimental scenario, the negative electrostatic gradient limits the overall diffusive/dispersive movement of positively charged ions and enhances the movement of the negatively charged ion.

This behavior is also evident from equations (1) and (9); in fact, for a cation, a negative electrical potential gradient leads to a migration flux component in the direction opposite to the diffusive/dispersive component and thus reduces its total flux. The situation is opposite for an anion where the same electrical potential gradient produces J_i^{mig} in the same direction as J_i^{dis} and consequently enhances the total transverse flux. Such behavior is also observed during the experiment as illustrated in the maps of fluxes in Figure 3.

In Scenario 2, the distribution of the net electrical potential gradient is significantly different compared to that of Scenario 1. In this experiment, $\frac{\partial \Phi}{\partial x_T}$ is negative in the outer fringe area whereas it is positive in the inner fringe of the ionic plume. The opposite behavior of $\frac{\partial \Phi}{\partial x_T}$ in these two fringe zones is clearly illustrated in Figure 6f. This outcome further explains the behavior observed in the flux maps in Figure 5, where the positive electromigration flux of the cations and the negative migration flux of the anion are induced by the positive electrical potential gradient in the inner fringe. However, in the outer fringe, $\frac{\partial \Phi}{\partial x_T}$ is negative and the situation is similar as in Scenario 1. Consequently, in this region, the negative electrostatic gradient retards the cations and accelerates the anion. The ions present in great excess (Mg^{2+} and Cl^-) have larger electrical gradient components compared to those of Scenario 1 (Figures 6c–6j). On the other
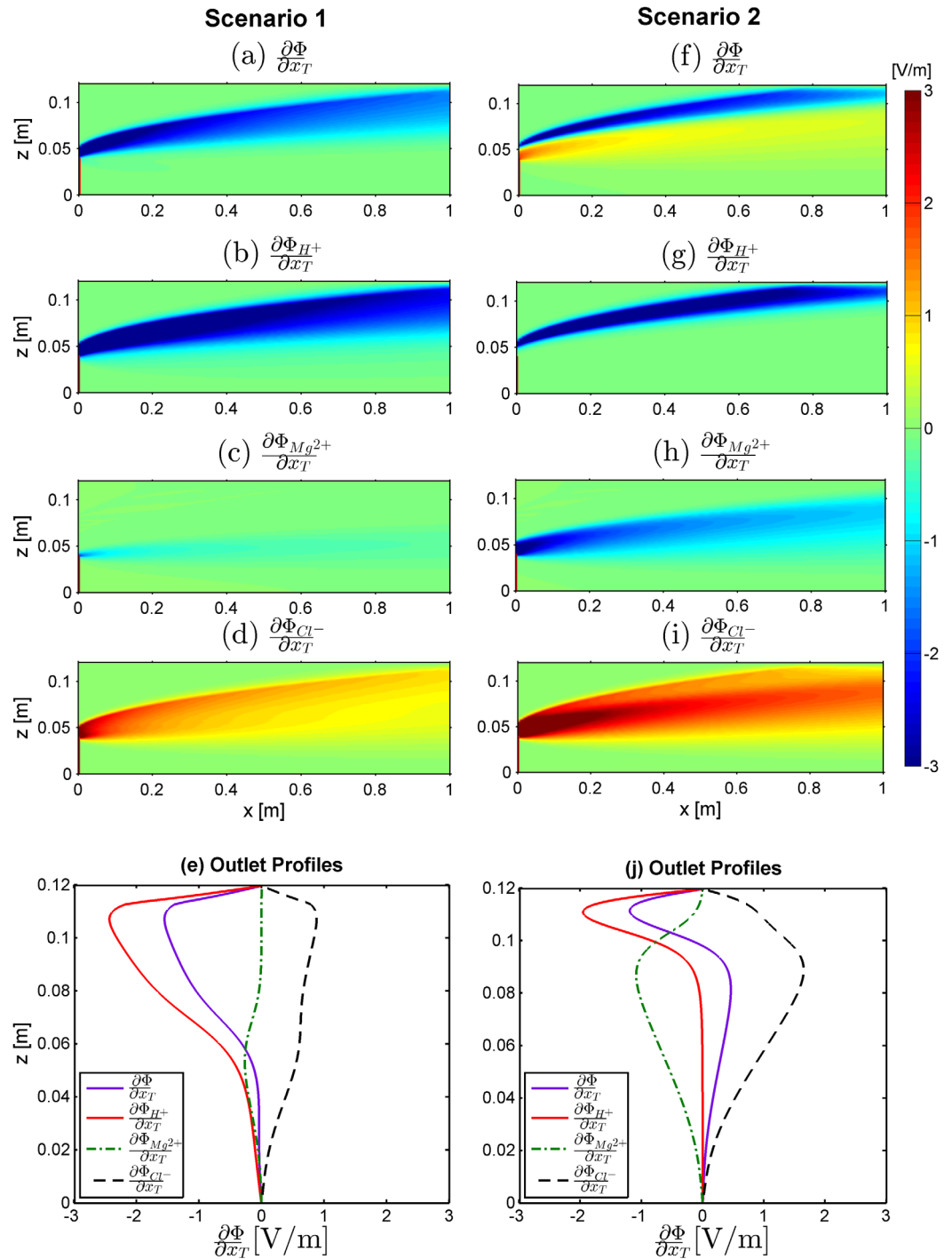
Figure 6. Maps of the transverse component of the electrostatic potential gradient produced during multicomponent ionic transport: the net electrical gradient (a, f), proton component (b, g), magnesium component (c, h), chloride component (d, i), and the outlet cross-sectional profiles (e, j) for Scenario 1 (Figures 6a–6e) and Scenario 2 (Figures 6f–6j).

hand, the proton component, $\frac{\partial \Phi_{H^+}}{\partial x_T}$ is around zero until the outer fringe ($z = \sim 8.5$ cm at the outlet), where it becomes negative (Figure 6j). Such behavior in the outlet cross-sectional profiles also implies that H$^+$ is the least involved species in the electrostatic coupling for most of the vertical cross section with the exception of the outer fringe area. However, in Scenario 1 the opposite is observed where H$^+$ is the most involved ion in the electrostatic coupling and major contributor to the net electrical potential gradient (Figure 6e).

5.4. Dilution of the Ionic Plumes

It is interesting to analyze the multicomponent transport problems and the flow-through experiments of this study using metrics of plume dilution. We use the flux-related dilution index [*Rolle et al.*, 2009] to quantify the dilution of the different ionic plumes due to their lateral displacement and mixing with deionized water. This metric, based on the concept of Shannon entropy, describes the distribution of a solute mass flux over the volumetric water flux at a given location along the main flow direction. The flux-related dilution index is particularly suited to study the dilution of solute plumes continuously emitted from a contamination source [*Chiogna et al.*, 2012; *Rolle et al.*, 2012]. For a multicomponent ionic transport problem, the flux-related dilution index of a charged species, i, reads as:

$$E_{Q,i}(x) = \exp\left(-\int_{\Omega} p_{Q,i}(\boldsymbol{x})\ln\left(p_{Q,i}(\boldsymbol{x})\right)q_x(\boldsymbol{x})d\Omega\right) \tag{12}$$

where $q_x = v\theta$ is the specific discharge in the main flow direction normal to the cross-sectional area Ω, θ is the porosity and $p_{Q,i}$ is the flux-related probability density function:

$$p_{Q,i}(\boldsymbol{x}) = \frac{C_i(\boldsymbol{x})}{\int_{\Omega} C_i(\boldsymbol{x})q_x(\boldsymbol{x})d\Omega} \tag{13}$$

The flux-related dilution index has been used as metric of plume dilution in both Stokes' and Darcy's flows [*Rolle et al.*, 2013b; *Rolle and Kitanidis*, 2014]. Physically $E_{Q,i}(x)$ represents an effective volumetric flux transporting the solute flux of a given ion i at the longitudinal position x. The values of $E_{Q,i}(x)$ monotonically increase with the travel distance in the flow-through system. For multicomponent transport, a higher value of the flux-related dilution index for a species i compared to the other ions in solution quantifies the higher dilution of the plume of that species. Figure 7 reports the computed flux-related dilution index, $E_{Q,i}$ at
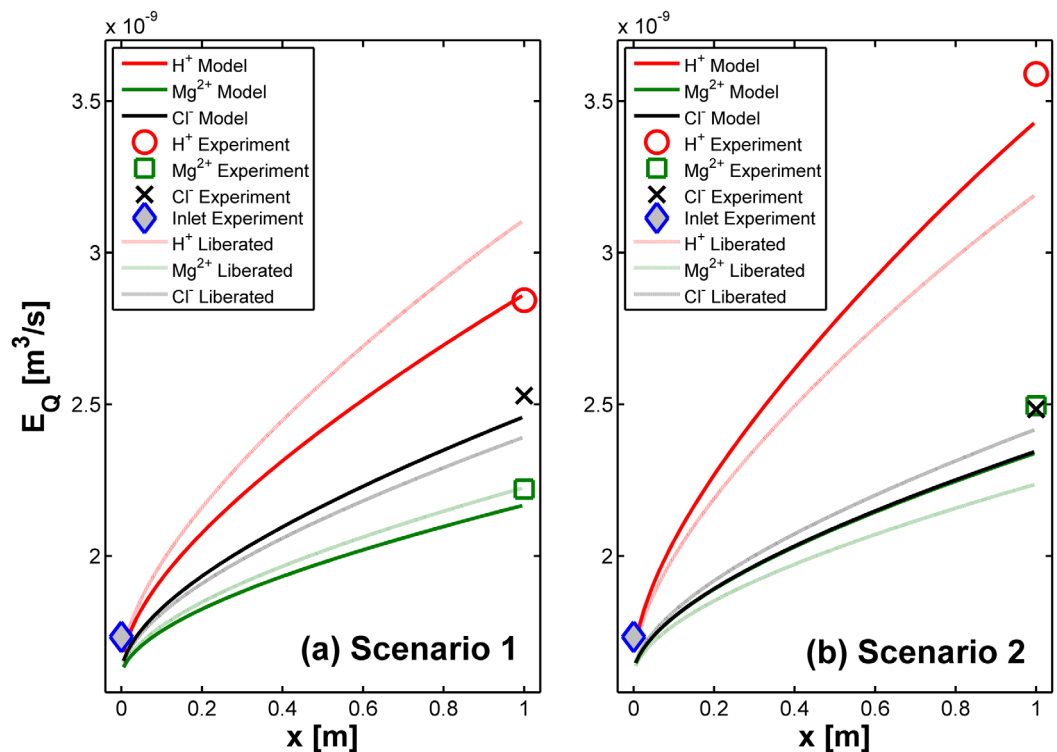

Figure 7. Observed (symbols) and simulated (lines) flux-related dilution index for the two experimental scenarios: (a) Scenario 1: injection of HCl and MgCl$_2$ with similar concentration (i.e., $C_{H+}/C_{Mg2+} \approx 1$) in Milli-Q water; (b) Scenario 2: injection of HCl and MgCl$_2$ with excess MgCl$_2$ concentration (i.e., $C_{H+}/C_{Mg2+} \approx 0.01$) in Milli-Q water. The term liberated refers to the case without electrostatic coupling (i.e., the species are transported as uncharged species with their own diffusive/dispersive properties).

different longitudinal cross sections for the investigated experimental scenarios. At the inflow boundary, the flux-related dilution index is identical for each ion because they are injected from the same inlet ports and thus show the same extent of dilution. However, E_Q profiles evolve differently for different ionic species in the porous media because the transported ions have different diffusive and dispersive properties leading to a distinct distribution of the ions' mass fluxes over the volumetric flux in the flow-through setup (Figures 7a and 7b).

The experimental flux-related dilution index, calculated from the concentrations and volumetric discharges measured at the inlet and outlet of the flow-through domain, shows a reasonable agreement with the model simulations. In Scenario 1, where two electrolytes (HCl and $MgCl_2$) were simultaneously injected at the same concentration level, all ions show distinct profiles that monotonically increase along the travel distance (Figure 7a). The dotted lines denote the simulated dilution of each species at their liberated state (i.e., as if they were transported as uncharged species). Both cations (H^+ and Mg^{2+}) show a reduction and the common anion (Cl^-) shows an enhancement of dilution compared to the case of displacement at liberated state conditions. In particular, the H^+ plume, although being clearly the most diluted one, shows a considerable decrease in the E_Q value compared to the outcomes of the multicomponent simulations describing H^+ undergoing transverse displacement according to its liberated state diffusive/dispersive properties. As discussed above, this limitation in dilution is due to the electrostatic interactions with the other charged species. This results in coupled dispersive fluxes that are caused by the development of an electrical potential gradient induced by the different diffusive rates of the ionic species in the solution (section 5.3) and by the dependence of local dispersion coefficients on the solutes' diffusivities, not only at slow but also at high flow velocities. The latter effect arises from incomplete mixing and compound-specific gradients of different solutes in the pore channels [*Rolle et al.*, 2012].

In Scenario 2, Mg^{2+} and Cl^- have identical profiles of flux-related dilution index and they also show practically the same measured values of E_Q (Figure 7b). This behavior is, in fact, induced from the composition of the injected electrolyte solution and the associated Coulombic cross-coupling of dispersive fluxes. Although $MgCl_2$ fully ionizes in solution, the cation and anion appear to travel together, nearly as a single salt. However, a close inspection of the concentrations of these ions reveals a tendency of Cl^- to displace slightly further in the transverse direction resulting in a small excess of Mg^{2+} in the core of the plume. This also affects the behavior of H^+ which tends to displace faster out of this region, thus receiving a positive electrostatic contribution to its lateral movement. As a result, the hydrogen ions displace at a rate that is even larger than the one expected under liberated state conditions. The enhanced displacement of H^+ results in a very dilute plume showing values of flux-related dilution index 45% higher than the other ionic species in the setup. Comparing the dilution of the H^+ plumes in the two experimental scenarios, it is interesting to notice that, based on the measured values at the outlet, the acidic plume in Scenario 2 is effectively distributed over a water flux which is 26% larger compared to the one carrying the acidic plume in Scenario 1. This outcome is quite striking since it shows that the extent of mixing for H^+ varies remarkably depending on the composition of the aqueous solution. This variation is solely due to the electrostatic Coulombic effects since both multicomponent ionic flow-through experiments were performed using the same electrolytes and under identical flow and transport conditions. The values of the flux-related dilution index measured at the outlet of the flow-through setup are summarized in Table 3.

5.5. Propagation of pH Fronts

As seen in the previous sections, the laboratory experiments with a ternary mixture of strong electrolytes have shown specific features of the concentration profiles of the different ions, the interaction of purely dispersive and electromigration fluxes as well a distinct dilution of the ionic plumes. Focusing on the proton displacement, the transport of H^+ in the saturated porous medium can be regarded and analyzed as a problem of propagation of dispersive pH fronts in the transverse direction. Figure 8 illustrates the results of the propagation of pH fronts for the two experimental scenarios. Figure 8a represents the vertical distances, beyond the injection zone, reached by the acidic fronts at different longitudinal cross sections in the flow-through setup. The calculation of

Table 3. Flux-Related Dilution Index Computed From Ion Concentrations and Volumetric Discharge Measured at the Outlet of the Flow-Through Setup

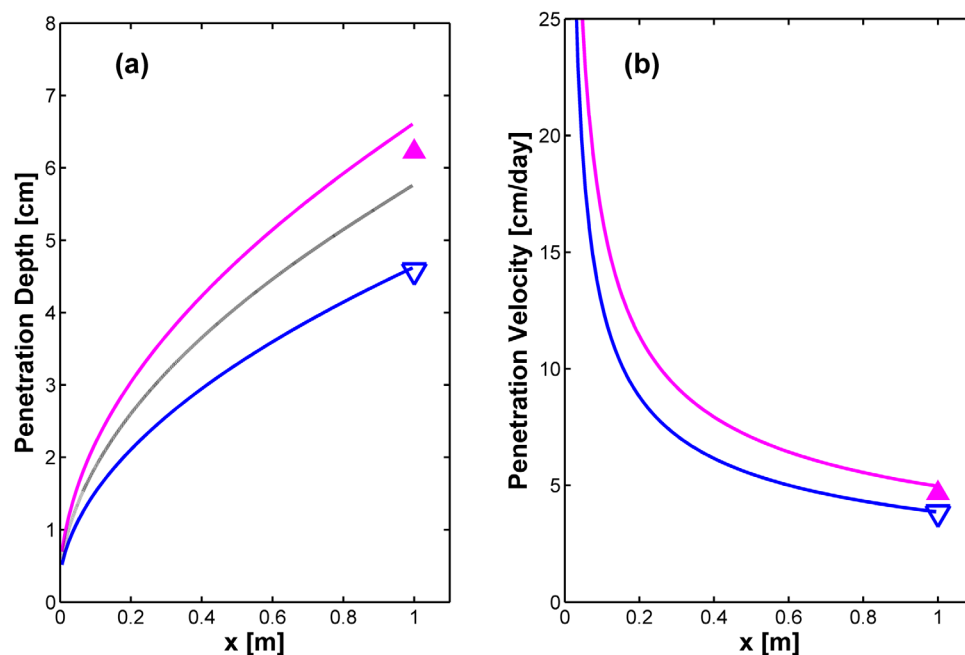| Ions	Flux-Related Dilution Index, $E_{Q,i}$ (m³/s)	
	Scenario 1	Scenario 2
H^+	2.84×10^{-9}	3.59×10^{-9}
Mg^{2+}	2.22×10^{-9}	2.50×10^{-9}
Cl^-	2.53×10^{-9}	2.48×10^{-9}

Figure 8. The symbols represents the observed (blue and pink colors for Scenario 1 and 2, respectively) penetration depths (a) and penetration velocities (b) of pH fronts in the two experimental scenarios. The lines are the simulated values including the case of penetration depth (black-dotted line) computed for liberated state (i.e., without electrostatic coupling). Penetration depth refers to the distance of pH front migration. The pH front is tracked considering a difference of 1.5 pH units from the initial solution pH.

such vertical distances, which can be regarded as a penetration depth traveled by the pH fronts, refers to changes of 1.5 units in pH compared to the inlet solution. These pH values were chosen as threshold for the edge of the acidic plumes.

Figure 8a clearly shows that the pH front at any longitudinal cross section migrates to a larger distance in Scenario 2 compared to Scenario 1. At the end of the flow-through domain ($x = 1$ m), the difference among the measured penetration depths in the two experimental scenarios reaches 1.6 cm. This behavior is consistent with the observations of the outlet pH profiles (Figures 2b and 4b) and of the flux-related dilution indices (Figure 7). The use of a different solution composition in Scenario 2 and the resultant Coulombic interactions between transported ionic species significantly accelerate the protons compared to the conditions tested in Scenario 1, thus causing a more effective penetration of the acidic front in Scenario 2. The different and increasing penetration depth of the acidic fronts at different cross sections along the water flow direction allow us to calculate a speed of propagation of the dispersive pH fronts in the vertical direction. The results are reported in Figure 8b and show distinct behaviors for the two experimental scenarios with faster propagation velocity of the pH front observed in Scenario 2. In both cases, the trend of such propagation velocities show that they reach their maximum close to the inlet of the flow-through setup, where due to the injection boundary conditions very high H^+ gradients occur. Due to hydrodynamic dispersion, those gradients tend to smooth along the water flow direction causing a reduced penetration velocity of the pH fronts at increasing longitudinal distances.

6. Summary and Conclusions

This study shows the significance of ionic interactions for the propagation of pH fronts in porous media. We have presented detailed flow-through experiments on multicomponent ionic transport in saturated porous media under steady-state conditions. In particular, we have studied the propagation of acidic fronts considering two distinct transport scenarios for mixed electrolyte solutions. Such experimental scenarios were chosen to demonstrate significantly different electromigration effects of the ions in solution on the transverse displacement of hydrogen ions, and thus on the propagation of dispersive pH fronts. The experiments have been quantitatively interpreted with a two-dimensional multicomponent ionic transport model based on an accurate description of local dispersion and accounting for charge conservation and for

electrochemical cross-coupling of charged species in the solution. Purely forward numerical simulations showed an excellent agreement with the high-resolution ion concentrations and pH profiles measured at the outlet of the laboratory setup.

The experimental and modeling results clearly show the importance of charge interactions and the cross-coupling of ion displacement also for advective-dispersive transport in porous media. Specifically, the effects of Coulombic interactions on acidic front migration were explored in this study and were shown to be particularly important for the propagation of pH fronts, since the displacement of hydrogen ions can be significantly accelerated or retarded depending on the concentration of other ions in solution. Considerable differences have been observed between the two experimental scenarios, both in terms of penetration depth of the pH fronts (relative difference of 36% between the two flow-through experiments) as well as for plume dilution (26% relative difference). Furthermore, the differences were also significant (up to 25% and 19% in penetration depth and plume dilution, respectively) compared to transport at liberated state (i.e., without considering the electrostatic cross-coupling). Coulombic interactions at the basis of multicomponent ionic transport occur at the small molecular scale; however, their effect propagates through the scales and impacts macroscopic solute transport. This was observed both in the flow-through experiments and from the outcomes of the numerical simulations. Furthermore, the conditions investigated highlight the importance of electromigration interactions not only at slow horizontal flow velocity but also for fast groundwater flow, under advection-dominated conditions. Two main factors contribute to these effects: the electrochemical coupling between different charged species and the incomplete mixing in the pore channels which is captured by macroscopic parameterizations of local transverse dispersion depending on solutes diffusivities not only at slow but also at high flow velocities [*Rolle et al.*, 2012; *Scheven*, 2013]. The latter effect has been proven to be relevant and to propagate also at larger field scales, in heterogeneous flow fields, provided that the spatial variability and dependence from the grain size of local dispersion coefficients is acknowledged [e.g., *Chiogna et al.*, 2011; *Eckert et al.*, 2012]. The experimental findings of this study also contribute to support the conclusions of recent investigations that pointed out the key role of aqueous diffusion for groundwater transport also at large scales [*LaBolle and Fogg*, 2008; *Rolle et al.*, 2013b; *Hadley and Newell*, 2014].

The effects of electromigration on pH front propagation, studied in this work under simplified conditions, can also impact more complex situations of subsurface flow and transport including transient transport conditions as well as additional physical and (bio)geochemical processes such as sorption, ion-exchange, surface complexation [e.g., *Gvirtzman and Gorelick*, 1991; *Zachara et al.*, 1991; *Bjerg and Christensen*, 1993; *Appelo*, 1994; *Liu et al.*, 2011; *Holden et al.*, 2012, 2013], geochemical weathering of sediments, pH buffering, release/mobilization of trace metals, mineral dissolution-precipitation, and degradation reactions [e.g., *Hansen and Postma*, 1995; *Kjøller et al.*, 2004; *Maher et al.*, 2006; *Tartakovsky et al.*, 2008; *Liu et al*, 2011; *Molins et al.*, 2012; *Li et al.*, 2014].

Finally, recent investigation of solute transport in homogeneous and heterogeneous three-dimensional experimental setups [*Ye et al.*, 2015a, 2015b] suggests that the charge interactions and the cross-coupling effects, studied in this work in (quasi) two-dimensional domains, would be even more pronounced for fully three-dimensional ionic transport in porous media.

References

Appelo, C. A. J. (1994), Cation and proton exchange, pH variations, and carbonate reactions in a freshening aquifer, *Water Resour. Res.*, *30*(10), 2793–2805.

Appelo, C. A. J., and P. Wersin (2007), Multicomponent diffusion modeling in clay systems with application to the diffusion of tritium, iodide, and sodium in opalinus clay, *Environ. Sci. Technol.*, *41*(14), 5002–5007.

Appelo, C. A. J., A. Vinsot, S. Mettler, and S. Wechner (2008), Obtaining the porewater composition of a clay rock by modeling the in- and out-diffusion of anions and cations from an in-situ experiment, *J. Contam. Hydrol.*, *101*(1–4), 67–76.

Appelo, C. A. J., L. R. Van Loon, and P. Wersin (2010), Multicomponent diffusion of a suite of tracers (HTO, Cl, Br, I, Na, Sr, Cs) in a single sample of Opalinus Clay, *Geochim. Cosmochim. Acta*, *74*(4), 1201–1219.

Bard, A. J., and L. R. Faulkner (2001), *Electrochemical Methods: Fundamentals and Applications*, 718 pp., John Wiley, N. Y.

Ben-Yaakov, S. (1972), Diffusion of sea water ions—I. Diffusion of sea water into a dilute solution, *Geochim. Cosmochim. Acta*, *36*(12), 1395–1406.

Bjerg, P. L., and T. H. Christensen (1993), A field experiment on cation exchange-affected multicomponent solute transport in a sandy aquifer, *J. Contam. Hydrol. 12*, 269–290.

Boudreau, B. P., F. J. R. Meysman, and J. J. Middelburg (2004), Multicomponent ionic diffusion in porewaters: Coulombic effects revisited, *Earth Planet. Sci. Lett.*, *222*(2), 653–666.

Chiogna, G., C. Eberhardt, P. Grathwohl, O. A. Cirpka, and M. Rolle (2010), Evidence of compound-dependent hydrodynamic and mechanical transverse dispersion by multitracer laboratory experiments, *Environ. Sci. Technol.*, *44*(2), 688–693.

Chiogna, G., O. A. Cirpka, P. Grathwohl, and M. Rolle (2011), Relevance of local compound-specific transverse dispersion for conservative and reactive mixing in heterogeneous porous media, *Water Resour. Res.*, *47*, W07540, doi:10.1029/2010WR010270.

Chiogna, G., D. L. Hochstetler, A. Bellin, P. K. Kitanidis, and M. Rolle (2012), Mixing, entropy and reactive solute transport, *Geophys. Res. Lett.*, *39*, L20405, doi:10.1029/2012GL053295.

Cirpka, O. A., E. O. Frind, and R. Helmig (1999a), Streamline-oriented grid generation for transport modelling in two-dimensional domains including wells, *Adv. Water Resour.*, *22*(7), 697–710.

Cirpka, O. A., E. O. Frind, and R. Helmig (1999b), Numerical methods for reactive transport on rectangular and streamline-oriented grids, *Adv. Water Resour.*, *22*(7), 711–728.

Cirpka, O. A., F. P. J. de Barros, G. Chiogna, M. Rolle, and W. Nowak (2011), Stochastic flux-related analysis of transverse mixing in two-dimensional heterogeneous porous media, *Water Resour. Res.*, *47*, W06515, doi:10.1029/2010WR010279.

Cussler, E. L. (2009), *Diffusion: Mass Transfer in Fluid Systems*, third ed., 631 pp., Cambridge Univ. Press, Cambridge, N. Y.

Davis, J. A., and D. B. Kent (1990), Surface complexation modeling in aqueous geochemistry, Eds. M.F. Hochella and A. F. White, Mineral-Water Interface Geochemistry, *Rev. Mineral.*, *23*, 177–260.

Davis, J. A., D. E. Meece, M. Kohler, and G. P. Curtis (2004), Approaches to surface complexation modeling of Uranium(VI) adsorption on aquifer sediments, *Geochim. Cosmochim. Acta*, *68*(18), 3621–3641.

Davis, T., and I. Duff (1997), An unsymmetric-pattern multifrontal method for sparse LU factorization, *SIAM J. Matrix Anal. A.*, *18*(1), 140–158.

de Caritat, P. (1995), Intensifying groundwater acidification at Birkenes, southern Norway, *J. Hydrol.*, *170*(1–4), 47–62.

Donovan, J. J., K. W. Frysinger, and T. P. Maher Jr. (1997), Geochemical response of acid groundwater to neutralization by alkaline recharge, *Aqaut. Geochem.*, *2*(3), 227–253.

Eckert, D., M. Rolle, and O. A. Cirpka (2012), Numerical simulation of isotope fractionation in steady-state bioreactive transport controlled by transverse mixing, *J. Contam. Hydrol.*, *140–141*(0), 95–106.

Edmunds, W.M., and D. G. Kinniburgh, (1986), The susceptibility of UK groundwaters to acidic deposition, *J. Geol. Soc.*, *143*, 707–720.

Engesgaard, P., and K. L. Kipp (1992), A geochemical transport model for redox-controlled movement of mineral fronts in groundwater flow systems: A case of nitrate removal by oxidation of pyrite, *Water Resour. Res.*, *28*(10), 2829–2843.

Fest, E. P. M. J., E. J. M. Temminghoff, J. Griffioen, and W. H. Van Riemsdijk (2005), Proton buffering and metal leaching in sandy soils, *Environ. Sci. Technol.*, *39*(20), 7901–7908.

Fest, E. P. M. J., E. J. M. Temminghoff, J. Griffioen, B. Grift, and W. H. Van Riemsdijk (2007), Groundwater chemistry of Al under Dutch acid sandy soils: Effects of land use and depth, *Appl. Geochem.*, *22*(7), 1427–1438.

Franken, G., D. Postma, W. H. M. Duijnisveld, J. Böttcher, and J. Molson (2009), Acid groundwater in an anoxic aquifer: Reactive transport modelling of buffering processes, *Appl. Geochem.*, *24*(5), 890–899.

Giambalvo, E. R., C. I. Steefel, A. T. Fisher, N. D. Rosenberg, and C. G. Wheat (2002), Effect of fluid-sediment reaction on hydrothermal fluxes of major elements, eastern flank of the Juan de Fuca Ridge, *Geochim. Cosmochim. Acta*, *66*(10), 1739–1757.

Griffioen, J. (1993), Multicomponent cation exchange including alkalinization/acidification following flow through sandy sediment, *Water Resour. Res.*, *29*(9), 3005–3019.

Gvirtzman, H., and S. M. Gorelick (1991), Dispersion and advection in unsaturated porous media enhanced by anion exclusion, *Nature*, *352*, 793–795.

Haberer, C. M., M. Rolle, O. A. Cirpka, and P. Grathwohl (2012), Oxygen transfer in a fluctuating capillary fringe, *Vadose Zone J.*, *11*(3).

Haberer, C. M., M. Muniruzzaman, P. Grathwohl, and M. Rolle (2015), Diffusive/Dispersive and reactive fronts in porous media: Fe (II)-oxidation at the unsaturated/saturated interface, *Vadose Zone J.*, *14*(5), doi:10.2136/vzj2014.07.0091.

Hadley, P. W., and C. Newell (2014), The new potential for understanding groundwater contaminant transport, *Groundwater*, *52*(2), 174–186.

Hansen, B. K., and D. Postma (1995), Acidification, buffering, and salt effects in the unsaturated zone of a sandy aquifer, Klosterhede, Denmark, *Water Resour. Res.*, *31*(11), 2795–2809.

Hochstetler, D. L., M. Rolle, G. Chiogna, C. M. Haberer, P. Grathwohl, and P. K. Kitanidis (2013), Effects of compound-specific transverse mixing on steady-state reactive plumes: Insights from pore-scale simulations and Darcy-scale experiments, *Adv. Water Resour.*, *54*, 1–10.

Holden, A. A., K. U. Mayer and A. C. Ulrich (2012), Evaluating methods for quantifying cation exchange in mildly calcareous sediments in Northern Alberta. *Appl. Geochem.*, *27*, 2511–2523.

Holden A. A., S. E. Haque, K. U. Mayer and A. C. Ulrich (2013) Biogeochemical processes controlling the mobility of major ions and trace metals in aquitard sediments beneath an oil sand tailing pond: Laboratory studies and reactive transport modeling, *J. Contam. Hydrol.*, *151*, 55–67.

Kent, D. B., R. H. Abrams, J. A. Davis, J. A. Coston, and D. R. LeBlanc (2000), Modeling the influence of variable pH on the transport of zinc in a contaminated aquifer using semiempirical surface complexation models, *Water Resour. Res.*, *36*(12), 3411–3425.

Kjøller, C., D. Postma, and F. Larsen (2004), Groundwater acidification and the mobilization of trace metals in a sandy aquifer, *Environ. Sci. Technol.*, *38*(10), 2829–2835.

LaBolle, E. M., and G. E. Fogg (2001), Role of molecular diffusion in contaminant migration and recovery in an alluvial aquifer system, *Transp. Porous Med.*, *42*(1-2), 155–179.

Lasaga, A. C. (1979), The treatment of multi-component diffusion and ion pairs in diagenetic fluxes, *Am. J. Sci.*, *279*(3), 324–346.

Lasaga, A. C. (1998), *Kinetic Theory in the Earth Sciences*, 811 pp., Princeton Univ. Press, Princeton, N. J.

Li, L., C. A. Peters, and M. A. Celia (2007), Effects of mineral spatial distribution on reaction rates in porous media, *Water Resour. Res.*, *43*, W01419, doi:10.1029/2005WR004848.

Li, L., C. I. Steefel, and L. Yang (2008), Scale dependence of mineral dissolution rates within single pores and fractures, *Geochim. Cosmochim. Acta*, *72*(2), 360–377.

Li, L., F. Salehikhoo, S. L. Brantley, and P. Heidari (2014), Spatial zonation limits magnesite dissolution in porous media, *Geochim. Cosmochim. Acta*, *126*(0), 555–573.

Liu, C. X. (2007), An ion diffusion model in semi-permeable clay materials, *Environ. Sci. Technol.*, *41*(15), 5403–5409.

Liu, C. X., J. M. Zachara, A. Felmy, and Y. Gorby (2004), An electrodynamics-based model for ion diffusion in microbial polysaccharides, *Colloids Surf. A and B*, *38*(1-2), 55–65.

Liu, C. X., J. Shang, and J. M. Zachara (2011), Multispecies diffusion models: A study of uranyl species diffusion, *Water Resour. Res.*, *47*, W12514, doi:10.1029/2011WR010575.

Maher, K., C. I. Steefel, D. J. DePaolo, and B. E. Viani (2006), The mineral dissolution rate conundrum: Insights from reactive transport modeling of U isotopes and pore fluid chemistry in marine sediments, *Geochim. Cosmochim. Acta*, *70*(2), 337–363.

Molins, S., D. Trebotich, C. I. Steefel, and C. P. Shen (2012), An investigation of the effect of pore scale flow on average geochemical reaction rates using direct numerical simulation, *Water Resour. Res.*, *48*, W03527, doi:10.1029/2011WR011404.

Moss, P. D., and W. M. Edmunds (1992), Processes controlling acid attenuation in the unsaturated zone of a Triassic sandstone aquifer (U.K.), in the absence of carbonate minerals, *Appl. Geochem.*, 7(6), 573–583.

Møller, K. B., R. Rey, M. Masia, and J. T. Hynes (2005), On the coupling between molecular diffusion and solvation shell exchange, *J. Chem. Phys.*, 122, 114,508,1–114,508,12.

Muniruzzaman, M., C. M. Haberer, P. Grathwohl, and M. Rolle (2014), Multicomponent ionic dispersion during transport of electrolytes in heterogeneous porous media: Experiments and model-based interpretation, *Geochim. Cosmochim. Acta*, 141(0), 656–669.

Parkhurst, D. L., and C. A. J. Appelo (1999), User's guide to PHREEQC - a computer program for speciation, reaction path, 1-D transport, and inverse geochemical calculations. *Tech. Rep. 99-4259*, US Geol. Survey Water Resources Investigation.

Prigiobbe, V., and S. L. Bryant (2014), pH-dependent transport of metal cations in porous media, *Environ. Sci. Technol.*, 48(7), 3752–3759.

Probstein, R. F. (1989), *Physicochemical Hydrodynamics: An Introduction*, 337 pp., Butterworth, Stoneham.

Redden, G., D. Fox, C. Zhang, Y. Fujita, L. J. Guo, and P. Huang (2014) CaCO3 precipitation, transport and sensing in porous media with in situ generation of reactants, *Environ. Sci. Technol.*, 48(1), 542–549.

Rolle, M., C. Eberhardt, G. Chiogna, O. A. Cirpka, and P. Grathwohl (2009), Enhancement of dilution and transverse reactive mixing in porous media: Experiments and model-based interpretation, *J. Contam. Hydrol.*, 110(3–4), 130–142.

Rolle, M., D. L. Hochstetler, G. Chiogna, P. K. Kitanidis, and P. Grathwohl (2012), Experimental investigation and pore-scale modeling interpretation of compound-specific transverse dispersion in porous media, *Transp. Porous Med.*, 93(3), 347–362.

Rolle, M., M. Muniruzzaman, C. M. Haberer, and P. Grathwohl (2013a), Coulombic effects in advection-dominated transport of electrolytes in porous media: Multicomponent ionic dispersion, *Geochim. Cosmochim. Acta*, 120, 195–205.

Rolle, M., G. Chiogna, D. L. Hochstetler, and P. K. Kitanidis (2013b), On the importance of diffusion and compound-specific mixing for groundwater transport: An investigation from pore to field scale, *J. Contam. Hydrol.*, 153, 51–68.

Rolle, M., and P. K. Kitanidis (2014), Effects of compound-specific dilution on transient transport and solute breakthrough: A pore-scale analysis, *Adv. Water Resour.*, 71, 186–19.

Scheven, U. M. (2013), Pore-scale mixing and transverse dispersivity of randomly packed monodisperse spheres, *Phys. Rev. Lett.*, 110, 214504.

Steefel, C. I., and K. Maher (2009), Fluid-rock interaction: A reactive transport approach, *Rev. Mineral. Geochem.*, 70, 485–532.

Tartakovsky, A.M., G. D. Redden, P. C. Lichtner, T. C. Scheibe, and P. Meakin (2008), Mixing-induced precipitation: Experimental study and multi-scale numerical analysis. *Water Resour. Res.*, 44, W06S04, doi:10.1029/2006WR005725.

Van Cappellen, P., and J. F. Gaillard (1996), Biogeochemical dynamics in aquatic sediments, *Rev. Mineral. Geochem.*, 34(1), 335–376.

Vinograd, J. R., and J. W. McBain (1941), Diffusion of electrolytes and of the ions in their mixtures, *J. Am. Chem. Soc.*, 63(7), 2008–2015.

Ye, Y., G. Chiogna, O. A. Cirpka, P. Grathwohl, and M. Rolle (2015a), Experimental investigation of compound-specific dilution of solute plumes in saturated porous media: 2-D vs. 3-D flow-through systems, *J. Contam. Hydrol.*, 172, 33–47.

Ye, Y., G. Chiogna, O. A. Cirpka, P. Grathwohl, and M. Rolle (2015b), Enhancement of plume dilution in two- and three-dimensional porous media by flow focusing in high-permeability inclusions, *Water Resour. Res.*, 51, doi:10.1002/2015WR016962, in press.

Zachara, J. M., C. E. Cowan, and C. T. Resch (1991), Sorption of divalent metals on calcite, *Geochim. Cosmochim. Acta*, 55(6), 1549–1562.